Pharmaceutical Sciences and Drug Design
ISSN: 3062-4428
2026, Volume 6, Issue 1, Page No: 86-105

Available online at: www.galaxypub.co/page/journals

Galaxy Publication

Galaxy Publication

Identification of Promising Xanthene, Coumarin, and Benzoxazole Scaffolds against SARS-CoV-2 Proteases via In Silico Screening

Hiroshi Tanaka[1], Yuki Sato[1]*, Kenji Mori[2], Rina Okabe[1], Takashi Ito[2]

[1]Department of Pharmaceutical Sciences and Drug Engineering, Faculty of Pharmacy, University of Tokyo, Tokyo, Japan.
[2]Department of Molecular Drug Design, Faculty of Pharmaceutical Sciences, Kyoto University, Kyoto, Japan.

***E-mail** ✉ yuki.sato@gmail.com

Received: 20 November 2025; **Revised:** 10 February 2026; **Accepted:** 11 February 2026

ABSTRACT

Even though COVID-19 is no longer considered a pandemic, SARS-CoV-2 continues to evolve through frequent mutations, giving rise to new variants and maintaining its relevance as a global public health concern. The lack of effective, orally available antiviral treatments complicates clinical management, underscoring the need to develop broad-spectrum antiviral agents capable of addressing current and future viral outbreaks. In this study, a molecular docking approach was applied to evaluate the binding interactions of 118 marine-derived compounds and 92 previously synthesized compounds with the SARS-CoV-2 main protease and papain-like protease. Compounds belonging to the xanthene, benzoxazole, and coumarin families were identified as the most promising candidates. Overall, marine-origin compounds exhibited a marginally stronger inhibitory potential against the target enzymes. However, synthetic compounds demonstrated comparable binding performance, with leading molecules showing affinities of 0.2-0.4 mM. Among all evaluated structures, xanthenes—present in both marine and synthetic libraries—emerged as the most favorable scaffolds for further optimization as enzyme inhibitors. In addition, the papain-like protease appeared to be more amenable to drug targeting than the main protease. All top-ranked compounds also fulfilled standard drug-likeness criteria, suggesting suitable oral bioavailability and a low probability of adverse pharmacological effects. Collectively, these findings offer comparative insights into the binding behaviors of marine-derived and synthetic xanthene, coumarin, and benzoxazole derivatives and identify lead candidates for subsequent in vitro and in vivo experimental validation.

Keywords: SARS-CoV-2, Marine origin compounds, Synthesized compounds, Docking

How to Cite This Article: Tanaka H, Sato Y, Mori K, Okabe R, Ito T. Identification of Promising Xanthene, Coumarin, and Benzoxazole Scaffolds against SARS-CoV-2 Proteases via In Silico Screening. Pharm Sci Drug Des. 2026;6(1):86-105 . https://doi.org/10.51847/p0FBDhVChU

Introduction

A novel severe acute respiratory syndrome coronavirus 2 (SARS-CoV-2) was first identified in Wuhan, China, in late 2019. Following its emergence, the virus spread rapidly worldwide, leading to coronavirus disease 2019 (COVID-19), a severe respiratory illness that has affected millions of individuals worldwide, with cases continuing to rise [1, 2]. On 11 March 2020, the World Health Organization (WHO) officially classified COVID-19 as a global pandemic. The infection has since reached nearly every country across all continents. However, reported case numbers likely underestimate the actual scale of infection due to limited testing capacity and a significant proportion of asymptomatic or mildly symptomatic cases that remain undetected or unreported. According to WHO statistics, as of 5 December 2024, there were 776,897,200 confirmed SARS-CoV-2 infections worldwide [3], including 7,076,329 associated deaths [4].

While COVID-19 is gradually shifting toward an endemic phase, SARS-CoV-2 continues to circulate globally and remains a persistent public health challenge. Newly emerging variants, characterized by extensive mutations in the spike protein, have been shown to evade neutralizing antibodies generated by vaccination or prior infection

[5]. This ongoing viral evolution reinforces the urgent need for broadly effective antiviral therapeutics capable of mitigating both current and future coronavirus outbreaks.

Coronaviruses are enveloped viruses containing single-stranded, positive-sense RNA genomes. Their name originates from the crown-like appearance observed under electron microscopy, which is caused by spike glycoproteins on the viral envelope surface [6]. These viruses belong to the family Coronaviridae, subfamily Orthocoronavirinae, within the order Nidovirales. The subfamily is divided into four genera: Alphacoronavirus, Betacoronavirus, Deltacoronavirus, and Gammacoronavirus [7]. Members of this viral family are known to infect a wide range of hosts. They are associated with respiratory, gastrointestinal, and neurological diseases in both humans and animals, such as camels, cats, and bats.

Coronaviruses can cross species barriers and cause diseases in humans ranging from mild upper respiratory tract infections, such as the common cold, to severe and potentially fatal conditions, including Middle East respiratory syndrome (MERS) and severe acute respiratory syndrome (SARS) [8]. SARS-CoV-2 is classified as a beta-coronavirus with a roughly spherical or oval morphology and a diameter of approximately 60 to 140 nm. It is sensitive to ultraviolet radiation and elevated temperatures [9]. Like other members of the coronavirus family, SARS-CoV-2 undergoes rapid evolutionary changes.

Therefore, viruses are not uniform entities but exist in multiple forms with diverse biological properties. Their genetic evolution occurs gradually over time spans ranging from months to years and can often be monitored and quantified. In the early phase of the outbreak, evolutionary changes were limited, and the D614G mutation became the globally dominant strain. This variant showed enhanced transmissibility, associated with comparatively mild disease severity [10]. However, ongoing mutations in the viral genome subsequently led to the appearance of numerous distinct variants [11, 12]. As a result, despite substantial global efforts in research, clinical management, and vaccine development for SARS-CoV-2, the overall risk to human health remains considerable [13]. The treatment of diseases caused by SARS-CoV-2—an RNA virus characterized by high transmissibility and rapid mutation—continues to pose a major global challenge, largely because of the limited availability of orally active antiviral drugs. This has encouraged the exploration of antiviral agents with alternative modes of action [14-16].

Two key viral enzymes, the main protease (Mpro) and the papain-like protease (PLpro), are indispensable for viral replication and therefore represent critical targets for drug discovery [17]. PLpro processes the viral polyproteins pp1a and pp1ab by cleaving them at three specific sites, producing the nonstructural proteins nsp1, nsp2, and nsp3, all of which are essential for viral propagation. It also disrupts host immune signaling by removing ubiquitin and ubiquitin-like interferon-stimulated gene 15 (ISG15) modifications from host proteins [18]. In contrast, Mpro is a cysteine protease characterized by a catalytic dyad formed by cysteine 145 (C145) and histidine 41 (H41) [19]. It targets host proteins such as interleukin-1 receptor-associated kinase 1 (IRAK1), TAK1-binding protein (TAB1), and mRNA-decapping enzyme 1A (DCP1A), thereby interfering with inflammatory cytokine production and weakening immune responses [20].

Despite both enzymes belonging to the family of nucleophilic cysteine proteases, they differ markedly in structural organization, catalytic mechanisms, and substrate specificity. Mpro primarily exists as a homodimer and relies on a Cys–His catalytic dyad to cleave the viral polyprotein at 11 distinct positions. PLpro, on the other hand, is generally monomeric and utilizes a Cys–His–Asp catalytic triad to cleave at the nsp1/2, nsp2/3, and nsp3/4 junctions [21]. PLpro shares structural similarity with certain human cysteine proteases, raising concerns about potential off-target effects during inhibitor development. In contrast, Mpro has no closely related human homologs, making it a more selective and safer pharmacological target for SARS-CoV-2 therapy [22]. Consequently, inhibiting the enzymatic function of Mpro and PLpro—which are essential for viral replication—offers a promising strategy for COVID-19 treatment by suppressing viral propagation, lowering viral load, and supporting host immune defense, thereby reducing disease severity [23].

Marine natural products constitute an important reservoir of bioactive molecules with significant pharmaceutical potential. These compounds exhibit a broad spectrum of biological activities, including antioxidant, antimicrobial, anti-inflammatory, anticoagulant, antidiabetic, anticancer, and immunomodulatory effects. They have been investigated for antiviral properties against coronaviruses, including SARS-CoV-2 and its major variants (e.g., Delta and Omicron), as well as against pathogens such as Mycobacterium tuberculosis, Helicobacter pylori, and HIV. Additionally, marine-derived compounds are being explored for their relevance in infection-associated cardiovascular diseases (irCVD), diabetes, and cancer [24].

Systematic evaluation of antiviral properties in known marine natural products can facilitate the prioritization of candidates for screening against SARS-CoV-2 in the search for new therapeutic or preventive strategies for

COVID-19. A wide range of antiviral molecules, effective against coronaviruses, has been identified from both marine and terrestrial sources [25]. Classes of marine-derived compounds such as flavonoids, phlorotannins, alkaloids, terpenoids, peptides, lectins, polysaccharides, lipids, and other secondary metabolites can interfere with multiple stages of the coronavirus life cycle, including viral entry, genome replication, and virion release, while also modulating host cellular pathways. These properties make them valuable candidates in antiviral drug development [26].

Several studies have confirmed that natural compounds possess inhibitory activity against SARS-CoV-2. Recent findings indicate that molecules belonging to the isoprenoid, peptide, polyketide, binaphthoquinone, and polyphenolic groups exhibit strong in vitro antiviral activity. Among compounds targeting the SARS-CoV-2 chymotrypsin-like protease (3CLpro)/main protease (Mpro) are dieckol, tannic acid, savinin, naringenin, esculetin-4-carboxylic acid ethyl ester, and amentoflavone [27, 28].

More recently, the repurposed marine-derived drug plitidepsin (dehydrodidemnin B, isolated from the ascidian *Aplidium albicans*) has been reported to exhibit antiviral potency more than 20 times higher than remdesivir against SARS-CoV-2 [29].

Other naturally occurring compounds with antiviral effects include stachyflin, active against influenza A virus [30]; topsentin and mycalamide, active against coronavirus A59 [31]; N-butyl harmine, which inhibits HIV replication [32]; tetrandrine, effective against human coronavirus OC43 [33]; saikosaponin B2, active against human coronavirus 229E [34]; and epigallocatechin gallate, which shows activity against SARS-CoV-2 [35]. In addition, three marine natural products—homofascaplysin A, (+)-aureole, and bromophycolide A—have been shown to inhibit SARS-CoV-2 replication at concentrations that are non-toxic to human airway epithelial cells. These compounds represent promising candidates for further development of novel antiviral agents [25].

In another investigation, new diketopiperazines (aspamides) and indolyl diketopiperazines were isolated from solid cultures of *Aspergillus versicolor*, an endophytic fungus associated with the sea crab (*Chiromantes haematocheir*), together with 11 previously known diketopiperazines and related intermediates. All isolated compounds were subjected to virtual screening against the SARS-CoV-2 3-chymotrypsin-like protease (Mpro). These compounds achieved the highest docking scores among all evaluated molecules, indicating strong potential as SARS-CoV-2 inhibitors [36]. Several additional studies have also been conducted to identify natural product-based inhibitors targeting SARS-CoV-2 [37-39].

Marine-derived natural products are considered to offer superior therapeutic benefits for the management of COVID-19 compared with conventional synthetic chemical drugs, some of which have been associated with adverse cardiovascular effects. The preservation of marine ecosystems is therefore essential for the sustainable advancement of the blue economy. As extensive, innovative, and highly promising sources of bioactive compounds for combating SARS-CoV-2 and infection-related cardiovascular diseases (irCVD), marine natural products may exert their effects through diverse mechanisms involving multiple molecular targets and signaling pathways that regulate immune responses and suppress inflammation [40].

In our earlier work, we have reported a wide range of syntheses, structural characterizations, and biological activities across several compound classes. For many years, our research has focused on 4-hydroxycoumarin derivatives, aryl-substituted xanthenes, and aryl-substituted benzoxazoles. In these investigations, molecular docking—a sophisticated computational technique used to predict ligand binding positions within target proteins—was extensively applied. We also frequently evaluated Lipinski's rule of five, which assesses the likelihood that synthesized compounds and potential drug candidates will exhibit oral bioavailability [41-43].

Building on this foundation, the SeaSAR v12 software was used to investigate 118 compounds derived from marine organisms, alongside 92 previously synthesized compounds, to evaluate their binding interactions with key SARS-CoV-2 enzymes, namely the main protease and the papain-like protease. Molecular docking served as a central computational method for predicting ligand–receptor binding modes and orientations within active sites. Furthermore, to assess the potential for oral administration, Lipinski's rule of five, additional drug-likeness parameters, and toxicity profiles were also considered. Compounds exhibiting the most favorable preliminary outcomes were subsequently selected for more in-depth computational evaluation.

Materials and Methods

Molecular docking simulations were conducted using SeeSAR v12.1 software (SeeSAR version 12.1; BioSolveIT GmbH, Sankt Augustin, Germany, 2022, www.biosolveit.de). Two SARS-CoV-2 protein structures were selected

as molecular targets: the main protease (PDB ID: 7ZQV) co-crystallized with the antiviral compound AG7404 (a rupintrivir-like inhibitor, AG7800), and the papain-like protease (PDB ID: 7TZJ) complexed with inhibitor 3k (a piperidine-based inhibitor).

A total of 118 marine-origin compounds with coumarin, xanthene, and benzoxazole scaffolds, along with 92 compounds from our internal library previously synthesized (comprising 56 xanthenes, 23 coumarins, 11 benzoxazoles, thymoquinone, and amino thymoquinone) [42-51], were selected and prepared as ligand structures. For comparative benchmarking, the FDA-approved SARS-CoV-2 Mpro inhibitor nirmatrelvir [52] and the experimental PLpro inhibitor Jun12682 [53] were included.

Docking parameters were maintained at their default settings within the SeeSAR platform. These default configurations are generally optimized to accommodate structurally diverse chemical libraries, including marine-derived natural products. Such compounds often exhibit high conformational flexibility, uncommon ring systems, and complex stereochemical features. In contrast, the synthesized compounds in this study tend to be more rigid, planar, and structurally less complex.

Binding affinity estimations were performed using the HYDE scoring function (Eq. 1) implemented in SeeSAR [54, 55]. Candidate compounds with the most favorable predicted affinities were selected for further analysis.

$$\Delta G_{Hyde} = \sum atom\ i \left[\Delta G^{f}_{dehydration} + \Delta G^{f}_{H-bonds}\right] \quad (1)$$

In Eq. (1), ΔGdehydration denotes the change in dehydration energy, while ΔGH-bonds represents the variation in hydrogen bond (H-bond) energy for each atom i within the protein–ligand complex. The HYDE scoring approach evaluates binding in terms of desolvation and hydration effects, parameters that are closely associated with octanol–water partition behavior. During ligand binding, complete dehydration of the ligand molecule is assumed.

The FlexX docking algorithm, integrated into SeeSAR, was used to position ligands within binding sites. This method is based on an incremental construction strategy [56, 57]. Ligands are initially decomposed into smaller fragments; the first fragment (or combinations of fragments) is positioned at multiple locations within the binding pocket using a rapid pre-scoring procedure. From a set of n initial solutions, ligands are then progressively reconstructed fragment by fragment, with intermediate conformations continuously ranked against one another. The highest-scoring docking poses are ultimately reported as the final output.

Physicochemical descriptors are among the key criteria used to evaluate whether a molecule is a viable drug candidate. Early prediction of ADME-related properties enables identification of potential toxicity risks and absorption limitations at the earliest stages of drug discovery, thereby improving efficiency and reducing developmental costs and time. In SeeSAR, the optional StarDrop (Optibrium) module is applied to estimate a broad set of molecular features, including the number of rotatable bonds, molecular weight, and topological polar surface area (TPSA), as well as pharmacokinetic descriptors such as CYP enzyme interaction potential, blood–brain barrier permeability (BBB), logS, and related ADME parameters. A full methodological description and references for these computed Optibrium descriptors are provided in the Optibrium Reference Guide, Optibrium Ltd., StarDrop, Waterbeach, UK, 2022 (www.optibrium.com).

Results and Discussion

A molecular docking-based virtual screening was performed to assess the binding affinities of 118 marine-origin compounds and 92 previously synthesized chemical entities. For comparative purposes, the FDA-approved SARS-CoV-2 main protease inhibitor nirmatrelvir was used as a reference standard, while jun12682 served as the benchmark compound for papain-like protease inhibition.

The docking outcomes of the most active marine-derived compounds **(Figure 1)** and synthetic compounds **(Figure 2)** against the SARS-CoV-2 main protease are summarized in **Tables 1 and 2.**

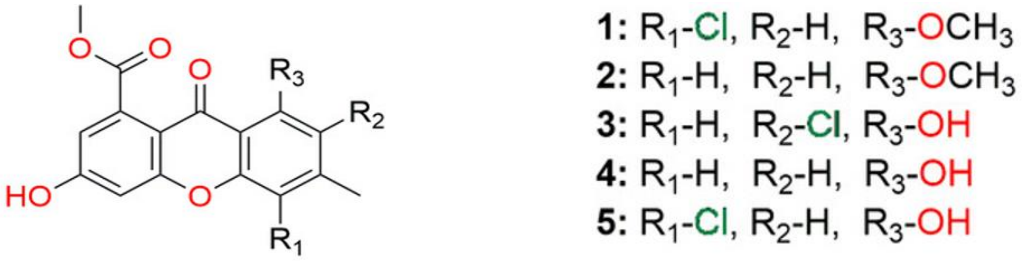

a) b)

Figure 1. Chemical scaffolds of the top-performing marine-origin compounds **(Table 1)** were evaluated against the main protease.

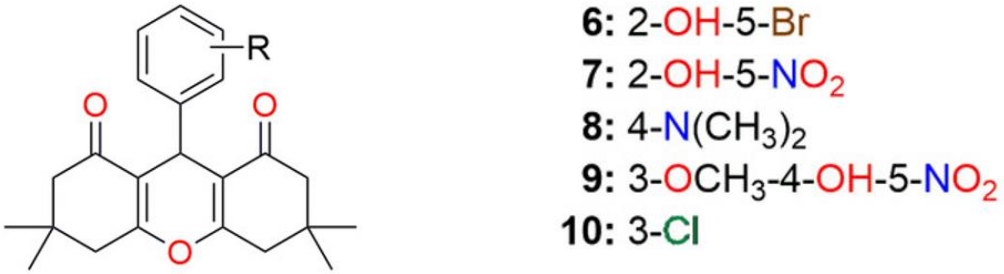

a) b)

Figure 2. Chemical scaffolds of the top-performing synthesized compounds **(Table 2)** were evaluated against the main protease.

Table 1. Docking outcomes and OPTIBRIUM-derived pharmacokinetic parameters for the five leading marine-origin compounds targeting SARS-CoV-2 main protease (PDB ID: 7ZQV).

DDP	Comp. (5)	Comp. (4)	Comp. (3)	Comp. (2)	Comp. (1)
L/U affinity [mM]	0.071/7.024	0.062/6.134	0.035/3.509	0.004/0.442	0.002/0.224
Mw (g/mol)	334.7	300.3	334.7	314.3	348.7
n H-acc.	5	5	5	5	5
n H-don.	2	2	2	1	1
n rot. bond	0	0	0	0	0
TPSA (Å²)	93.1	93.1	93.1	82.1	82.1
logP	3.86	3.33	3.78	2.93	3.50
logD	1.50	1.01	1.56	2.93	3.50
logS @ pH 7.4	3.88	3.98	3.90	2.19	1.36
HIA	+	+	+	+	+
BBB	-	-	-	-	-
PPB90	High	High	High	High	High
2C9 pKi	5.44	5.28	5.48	5.46	5.66
2D6	Medium	Medium	Medium	Medium	Medium
P-gp	No	No	No	No	No
hERG pIC_{50}	4.94	4.79	4.81	5.07	5.23

DDP—docking and drug-likeness descriptors; Comp. (1)—1-acetoxy-5-chloro-3-hydroxy-8-methoxy-6-methylxanthen-9-one; Comp. (2)—1-acetoxy-3-hydroxy-8-methoxy-6-methylxanthen-9-one; Comp. (3)—1-acetoxy-7-chloro-3,8-dihydroxy-6-methylxanthen-9-one; Comp. (4)—1-acetoxy-3,8-dihydroxy-6-methylxanthen-9-one; Comp. (5)—1-acetoxy-5-chloro-3,8-dihydroxy-6-methylxanthen-9-one; L/U affinity—predicted lower and upper affinity range; Mw—molecular weight; n H-acc.—hydrogen bond acceptor count; n H-don.—hydrogen bond donor count; n rot. bonds—number of rotatable bonds; TPSA—topological polar surface area; logP—lipophilicity index; logD—distribution coefficient; logS @ pH7.4—aqueous solubility at physiological pH; HIA—human intestinal absorption prediction; BBB—blood–brain barrier penetration; PPB90—plasma protein binding; 2C9 pKi—logarithmic CYP2C9 inhibition constant; 2D6—CYP2D6 substrate prediction; P-gp—P-glycoprotein substrate prediction; hERG pIC50—predicted hERG inhibition potency.

Table 2. Docking outcomes and OPTIBRIUM-derived pharmacokinetic parameters for the five leading synthesized compounds targeting SARS-CoV-2 main protease (PDB ID: 7ZQV).

DDP	Comp. (10)	Comp. (9)	Comp. (8)	Comp. (7)	Comp. * (6)
L/U affinity [mM]	0.046/4.594	0.019/1.904	0.012/1.211	0.008/0.747	0.005/0.473
Mw (g/mol)	384.9	441.5	393.5	411.5	445.4
n H-acc.	3	7	3	6	4
n H-don.	0	1	0	1	1
n rot. bond	1	1	1	1	1
TPSA (Å²)	43.4	118.7	46.6	109.4	63.6
logP	5.00	3.88	4.52	3.99	4.70
logD	5.00	3.88	2.58	3.99	4.70
logS @ pH 7.4	0.10	−0.06	2.10	0.75	0.80
HIA	+	+	+	+	+
BBB	+	-	+	-	+
PPB90	High	High	High	High	High
2C9 pKi	5.29	5.32	5.20	5.27	5.34
2D6	High	High	High	High	High
P-gp	No	Yes	Yes	Yes	Yes
hERG pIC_{50}	4.83	4.44	5.24	4.79	4.96

Complete structural description of xanthene derivatives: 3,3,6,6-tetramethyl-9-(substituted)phenyl-3,4,5,6,7,9-hexahydro-1H-xanthene-1,8(2H)-dione. DDP—docking and drug-likeness descriptors; Comp. (6)—9-(5-bromo-2-hydroxyphenyl)xanthen-1,8-dione; Comp. (7)—9-(2-hydroxy-5-nitrophenyl)xanthen-1,8-dione; Comp. (8)—19-(4-dimethylaminophenyl)xanthen-1,8-dione; Comp. (9)—9-(4-hydroxy-3-methoxy-5-nitrophenyl)xanthen-1,8-dione; Comp. (10)—9-(3-chlorophenyl)xanthen-1,8-dione; L/U affinity—estimated lower/upper binding limits; Mw—molecular weight; n H-acc.—hydrogen bond acceptors; n H-don.—hydrogen bond donors; n rot. bonds—rotatable bond count; TPSA—topological polar surface area; logP—lipophilicity; logD—distribution coefficient; logS @ pH7.4—solubility at physiological pH; HIA—intestinal absorption prediction; BBB—blood–brain barrier permeability; PPB90—plasma protein binding; 2C9 pKi—CYP2C9 inhibition constant (log scale); 2D6—CYP2D6 substrate prediction; P-gp—P-glycoprotein interaction; hERG pIC50—hERG channel inhibition index.

Docking results indicated that the predicted binding affinity range (lower/upper limit) for nirmatrelvir **(Figure 3)** was 2.448/243.213 mM.

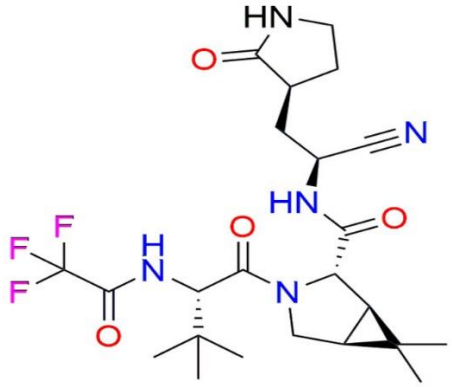

Figure 3. Molecular structure of nirmatrelvir.

Although classified as an FDA-approved inhibitor of Mpro, nirmatrelvir surprisingly exhibited significantly weaker predicted binding affinity—approximately 500-fold lower than compound 6 and nearly 1200-fold lower than compound 1.

The docking results for the most active marine-derived **(Figure 4)** and synthesized compounds **(Figure 5)** against SARS-CoV-2 papain-like protease are presented in **Tables 3 and 4.**

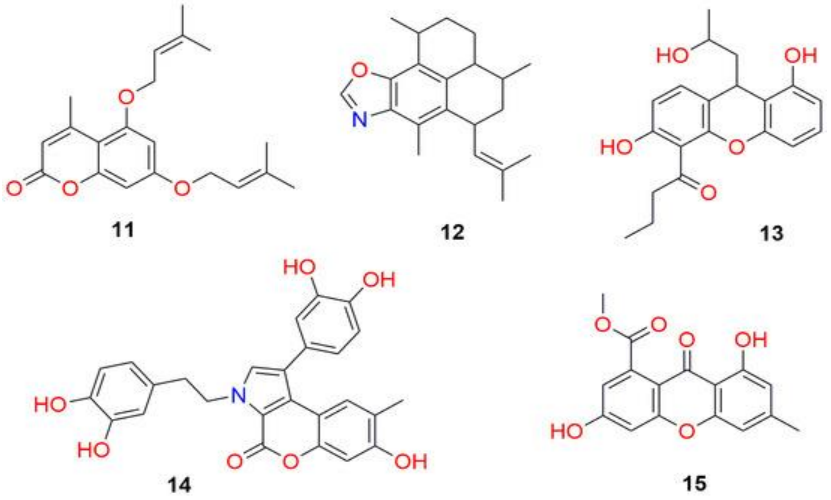

Figure 4. Chemical structures of the top marine-origin compounds **(Table 3)** were evaluated against papain-like protease.

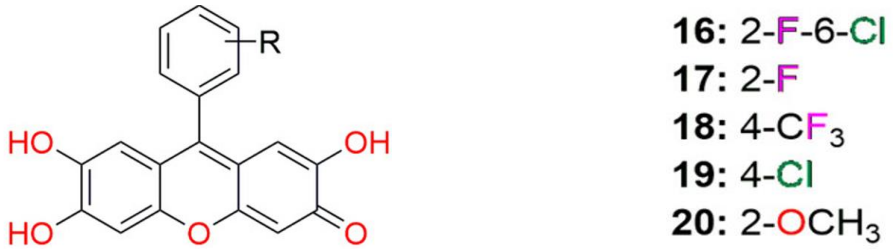

a) b)

Figure 5. Chemical structures of the top synthesized compounds **(Table 4)** were evaluated against papain-like protease.

Table 3. Docking outcomes and OPTIBRIUM-derived pharmacokinetic parameters for the five leading marine-origin compounds targeting SARS-CoV-2 papain-like protease (PDB ID: 7TZJ).

DDP	Comp. (15)	Comp. (14)	Comp. (13)	Comp. (12)	Comp (11)
L/U affinity [mM]	0.005/0.483	0.004/0.431	0.003/0.341	0.003/0.299	0.0001/0.010
Mw (g/mol)	300.3	461.4	342.4	309.4	328.4
n H-acc.	5	8	4	2	4
n H-don.	2	6	3	0	0
n rot. bond	0	3	4	1	4
TPSA (Å^2)	93.06	152.61	86.99	26.03	44.76
logP	3.33	2.51	3.82	6.46	4.28
logD	1.01	2.51	3.82	6.46	4.28
logS @ pH 7.4	3.98	2.39	1.55	0.57	1.08
HIA	+	-	+	+	+
BBB	-	-	-	+	+
PPB90	High	Low	High	High	High
2C9 pKi	5.28	5.83	5.33	5.23	4.86
2D6	Medium	Medium	High	Very high	Medium
P-gp	No	Yes	Yes	Yes	No
hERG pIC$_{50}$	4.79	5.70	5.07	6.06	5.74

DDP—docking and drug-likeness descriptors; Comp. (11)—4-methyl-5,7-bis((3-methylbut-2-en-1-yl)oxy)coumarin; Comp. (12)—pseudopteroxazole; Comp. (13)—5-(butan-1-onyl)-1,6-dihydroxy-9-(2-hydroxypropyl)xanthene; Comp. (14)—3-(3,4-dihydroxy phenethyl)-1-(3,4-dihydroxyphenyl)-7,8-dihydroxychromeno[3,4-b]pyrrol-4(3H)-one; Comp. (15)—1-acetoxy-3,8-dihydroxy-6-methylxanthen-9-one; L/U affinity—predicted binding range (lower/upper limits); Mw—molecular weight; n H-acc.—hydrogen bond

acceptors; n H-don.—hydrogen bond donors; n rot. bonds—rotatable bond count; TPSA—topological polar surface area; logP—lipophilicity index; logD—distribution coefficient; logS @ pH7.4—aqueous solubility at physiological pH; HIA—human intestinal absorption prediction; BBB—blood–brain barrier penetration; PPB90—plasma protein binding; 2C9 pKi—CYP2C9 inhibition constant (log scale); 2D6—CYP2D6 substrate prediction; P-gp—P-glycoprotein substrate status; hERG pIC50—predicted hERG inhibitory activity.

Table 4. Docking outcomes and OPTIBRIUM-based descriptors for the five leading synthesized compounds targeting SARS-CoV-2 papain-like protease (PDB ID: 7TZJ).

DDP	Comp. (20)	Comp. (19)	Comp. (18)	Comp. (17)	Comp. (16)
L/U affinity [mM]	0.0029/0.286	0.0025/0.246	0.0024/0.242	0.0023/0.223	0.0017/0.171
Mw (g/mol)	350.3	354.7	388.3	338.3	372.7
n H-acc.	1	0	2	1	2
n H-don.	5	4	4	4	4
n rot. bond	3	3	3	3	3
TPSA (Å^2)	96.22	86.99	86.99	86.99	86.99
logP	3.23	3.95	3.83	3.46	3.90
logD	3.23	3.95	3.83	3.46	3.90
logS @ pH 7.4	2.59	2.46	2.21	2.51	2.07
HIA	+	+	+	+	+
BBB	-	-	-	-	-
PPB90	Low	High	High	High	High
2C9 pKi	5.92	5.99	6.14	5.96	6.04
2D6	Low	Low	High	Low	Low
P-gp	No	No	No	No	No
hERG pIC$_{50}$	4.81	4.99	5.20	5.06	5.03

DDP—docking and drug-likeness descriptors; Comp. (16)—9-(2-fluoro-6-chlorophenyl)-2,6,7-trihydroxyxanthen-3-one; Comp. (17)—9-(2-fluorophenyl)-2,6,7-trihydroxyxanthen-3-one; Comp. (18)—9-(4-trifluoromethylphenyl)-2,6,7-trihydroxy xanthen-3-one; Comp. (19)—9-(4-chlorophenyl)-2,6,7-trihydroxy xanthen-3-one; Comp. (20)—9-(2-methoxy phenyl)-2,6,7-trihydroxyxanthen-3-one; L/U affinity—predicted lower and upper binding limits; Mw—molecular weight; n H-acc.—hydrogen bond acceptor count; n H-don.—hydrogen bond donor count; n rot. bonds—rotatable bond number; TPSA—topological polar surface area; logP—lipophilicity; logD—distribution coefficient; logS @ pH7.4—aqueous solubility at pH 7.4; HIA—human intestinal absorption; BBB—blood–brain barrier permeability; PPB90—plasma protein binding; 2C9 pKi—logarithmic CYP2C9 inhibition constant; 2D6—CYP2D6 substrate prediction; P-gp—P-glycoprotein substrate; hERG pIC50—hERG channel inhibition parameter.

As no clinically approved inhibitor exists for SARS-CoV-2 PLpro, the experimental molecule Jun12682 **(Figure 6)** was used as a reference for benchmarking. Docking calculations yielded a predicted affinity range (lower/upper boundary) of 2.173/215.899 mM. Notably, this reference compound exhibited markedly weaker binding toward PLpro when compared with both marine-derived and synthetically prepared ligands investigated in this work.

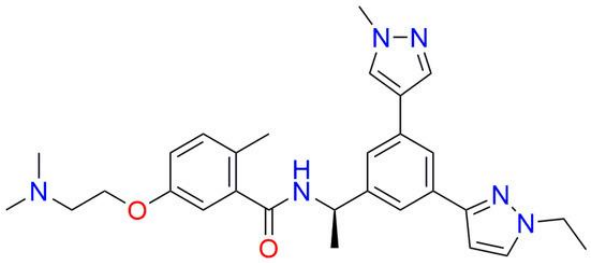

Figure 6. Chemical structure of Jun12682.

Due to the large number of evaluated compounds, the discussion is limited to the five highest-ranking molecules for each enzyme target and ligand category, focusing on binding strength and drug-likeness.

Docking results for the SARS-CoV-2 main protease (PDB ID: 7ZQV) revealed clear patterns in ligand recognition. All five top-performing marine-origin compounds were identified as xanthene-based structures. These scaffolds are derived from a 2-hydroxy-4-acetoxy-7-methylxanthen-9-one core and appear in multiple modified forms, including substitutions with 5-hydroxy or 5-methoxy groups, as well as chloro substituents at positions 6 or 8 **(Figures 1, 7 and 8).**

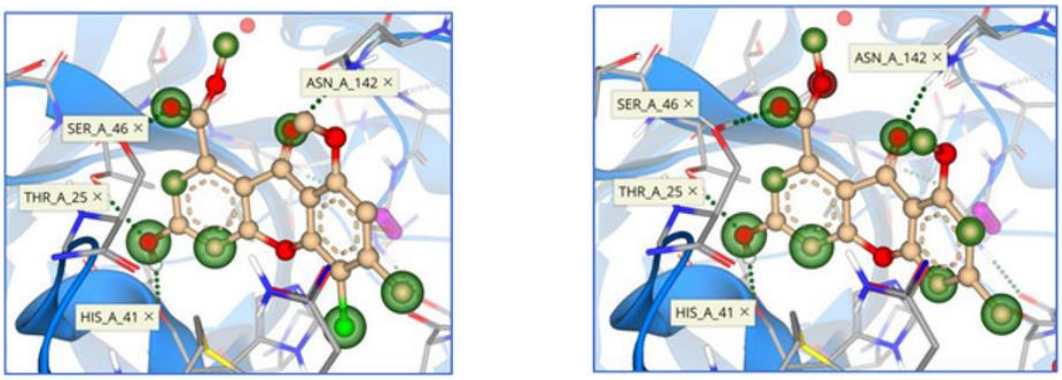

a) b)

Figure 7. Binding conformations and interacting residues of compounds 1 (a) and 2 (b) in the SARS-CoV-2 main protease active site, including atom-wise HYDE energy contributions to binding affinity (green highlighted atoms).

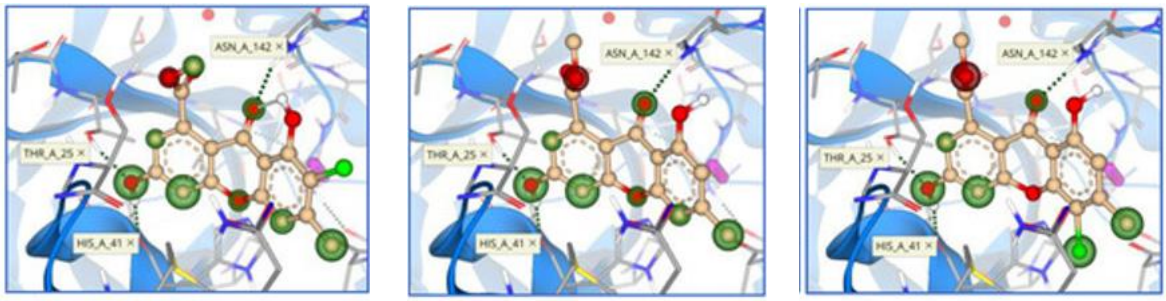

a) b) c)

Figure 8. Binding conformations and interacting residues of marine compounds 3 (a), 4 (b), and 5 (c) within the main protease binding pocket, with HYDE-based atomic contribution mapping (green highlighted atoms).

Predicted upper affinity limits (mM) for the first two compounds were tightly clustered between 0.224 and 0.442, whereas compound 3 and all subsequent analogs showed a pronounced drop in binding performance, exceeding values of 3.5 mM **(Table 1).** This nearly order-of-magnitude loss in affinity was unexpected given their close structural resemblance. However, the trend suggests that substitution at position 5—particularly methoxy functionality in the most active derivatives—is a key determinant of binding strength.

In addition, chlorine substitution was observed in three of the five best-performing molecules, suggesting a contributory role of halogen atoms in stabilizing interactions within the main protease binding site.

Frequent contact residues across all ligand–protein complexes included Thr 25, His 41, Ser 46, and Asn 142 **(Figures 7 and 8).** A particularly consistent interaction observed across all compounds was hydrogen bonding between the 2-hydroxy group and His41, a residue that forms part of the enzyme's catalytic dyad.

In the structural representations, the HYDE analysis quantifies atomic contributions to binding affinity (green circles denote favorable contributions), with larger circles indicating stronger energetic contributions. Red-marked atoms indicate unfavorable energetic effects opposing binding.

Among the top 20 ranked derivatives, additional relevant scaffolds include coumarin derivatives and fused coumarin systems incorporating furan and pyrrole rings. Notably, none of the evaluated benzoxazole derivatives were included in this top-ranked subset.

Docking analysis of synthesized xanthene, coumarin, and benzoxazole derivatives against the main protease indicated a clear dominance of 9-aryl-substituted xanthene-1,8-dione scaffolds among the best-performing compounds **(Figures 2, 9 and 10).**

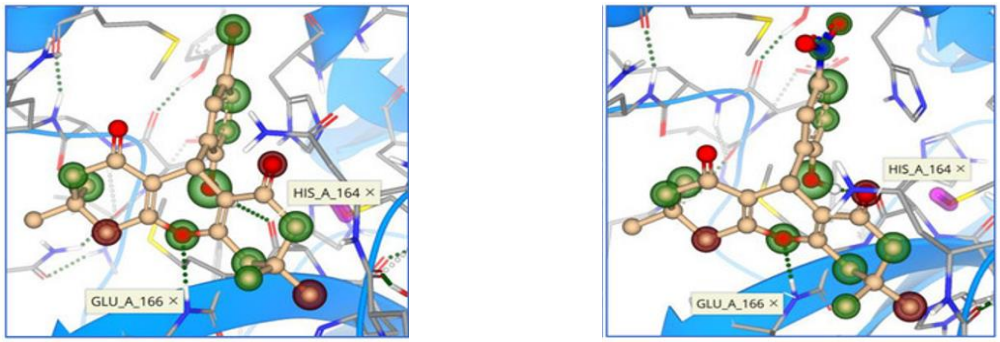

a) b)

Figure 9. Binding conformations and interacting residues of synthesized compounds 6 (a) and 7 (b) within the SARS-CoV-2 main protease binding pocket, with HYDE atomic contribution visualization (green highlighted atoms).

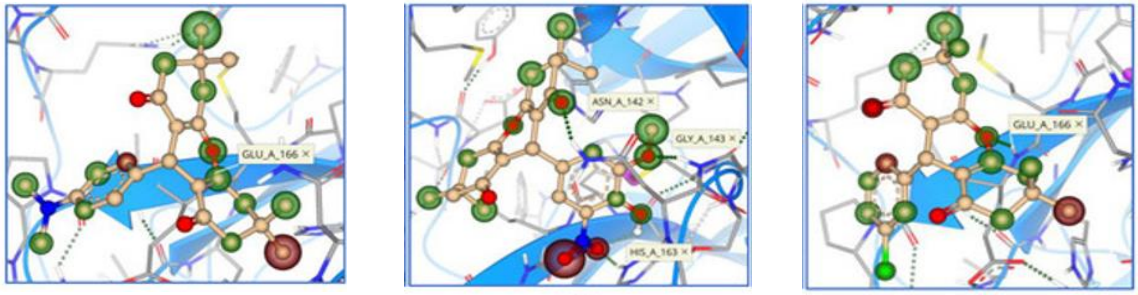

a) b) c)

Figure 10. Binding conformations and interacting residues of synthesized compounds 8 (a), 9 (b), and 10 (c) in the main protease active site, including HYDE-based energetic contribution mapping (green highlighted atoms).

Among the 20 top-scoring derivatives reported, the majority—14 compounds—are classified as xanthene-1,8-dione derivatives, while the remaining 6 belong to the 3-cinnamoyl-4-hydroxycoumarin family. A key structural distinction is observed between these groups and xanthene-3-one derivatives: the latter possess a rigid planar xanthene core, whereas xanthene-1,8-diones adopt a non-planar, bent tricyclic architecture. This conformational deviation introduces additional flexibility, which appears to enhance accommodation within the main protease binding pocket and may account for their improved binding affinity profiles.

For coumarin-based compounds, the heterocyclic core remains essentially planar; however, this scaffold is inherently smaller than that of xanthene systems. The presence of a 3-cinnamoyl substituent introduces conformational mobility, increasing structural adaptability relative to the rigid coumarin ring. This balance between rigidity and flexibility likely enables these molecules to align effectively within the enzymatic active site, supporting stable interactions.

Within the synthesized compound library, only a single derivative—9-(5-bromo-2-hydroxyphenyl)-3,3,6,6-tetramethylxanthene-1,8(2H)-dione—achieved binding affinity comparable to marine-derived molecules, with a value of 0.473 mM. The other four synthesized analogs were substantially weaker, each exceeding 0.747 mM, representing at least a twofold reduction in potency **(Table 2).**

In contrast to marine-origin ligands, the synthesized xanthene-1,8-diones did not form interactions with the catalytic His41 residue. Their interaction profiles were instead dominated by residues Asn 142, Gly 143, Ser 144, His 163, His 164, and Glu 166 **(Figures 9 and 10).**

Overall ranking data indicate that synthesized xanthen-3-one and benzoxazole derivatives were generally less competitive in receptor binding affinity compared with the leading compound groups discussed earlier.

Docking simulations against SARS-CoV-2 papain-like protease (PDB ID: 7TZJ) produced a chemically diverse set of top five marine-origin hits **(Table 3).** This subset includes two coumarin-based compounds, two xanthene derivatives, and one benzoxazole scaffold **(Figure 4).** Several of these structures also incorporate fused or extended cyclic systems appended to the core framework. Binding analysis revealed frequent interactions with Asp 164, Arg 166, Tyr 264, Gly 266, and Tyr 268 **(Figures 11 and 12).**

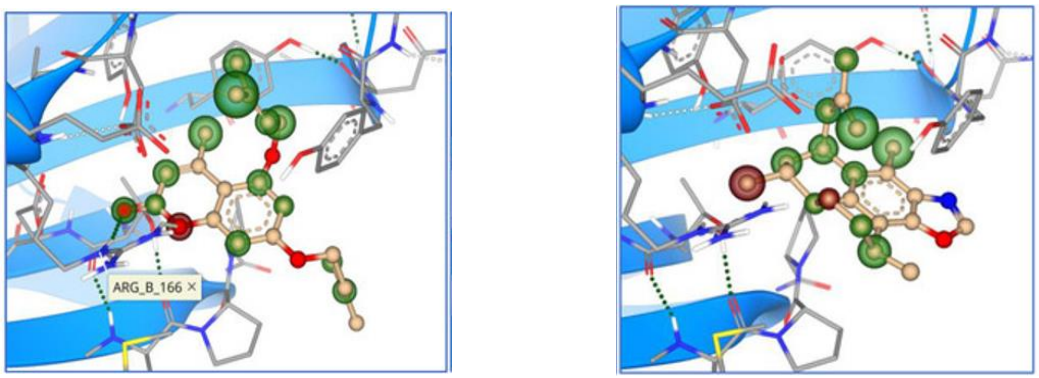

a) b)

Figure 11. Binding conformations and interacting amino acid residues of marine compounds 11 (a) and 12 (b) within papain-like protease, including HYDE atom-level energetic contributions (green circled atoms).

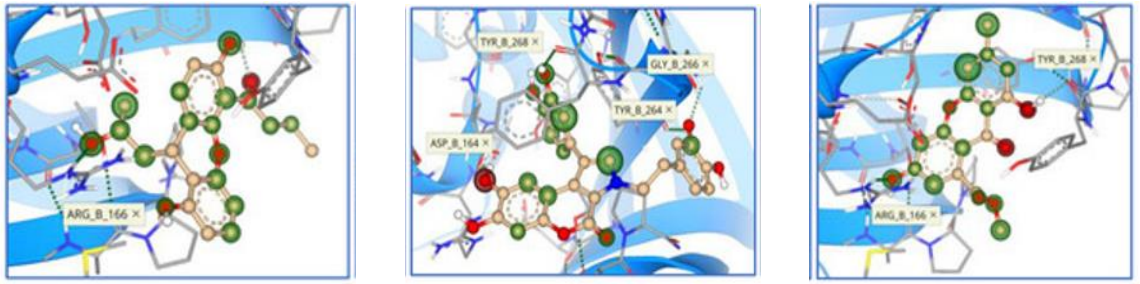

a) b) c)

Figure 12. Binding conformations and interacting amino acid residues of marine compounds 13 (a), 14 (b), and 15 (c) within papain-like protease, with HYDE-based atomic contribution visualization (green circled atoms).

The strongest inhibitor identified in this set was 4-methyl-5,7-bis((3-methylbut-2-en-1-yl)oxy)coumarin **(Figures 4 and 11)** compound 11, which displayed an exceptionally low upper-bound affinity of 0.01 mM. This corresponds to an estimated ~30-fold increase in potency relative to the remaining candidates.

The other four compounds exhibited affinity values between 0.299 and 0.483 mM, collectively indicating that papain-like protease is more readily targeted and more pharmacologically accessible to this compound library than the main protease. Additionally, 2,5-dihydroxy-4-acetoxy-7-methylxanthen-9-one **(Figure 4),** (compound 15), identified among the top PLpro hits **(Table 3),** also appeared in the top five Mpro-active compounds **(Table 1)**, (compound 4). Although its affinity varies between the two enzymes, it represents the only compound in this dataset with dual-target potential.

In contrast to the behavior observed with synthesized compounds against the main protease **(Table 2),** PLpro inhibition was dominated by 9-aryl-substituted derivatives of 2,6,7-trihydroxyxanthen-3-one, which feature a planar xanthene backbone. Structural diversity within this group arises mainly from substitutions at the 9-position of the aromatic ring **(Figures 5, 13 and 14).** Among the five leading candidates, four contain halogen substituents, while only one incorporates a methoxy group.

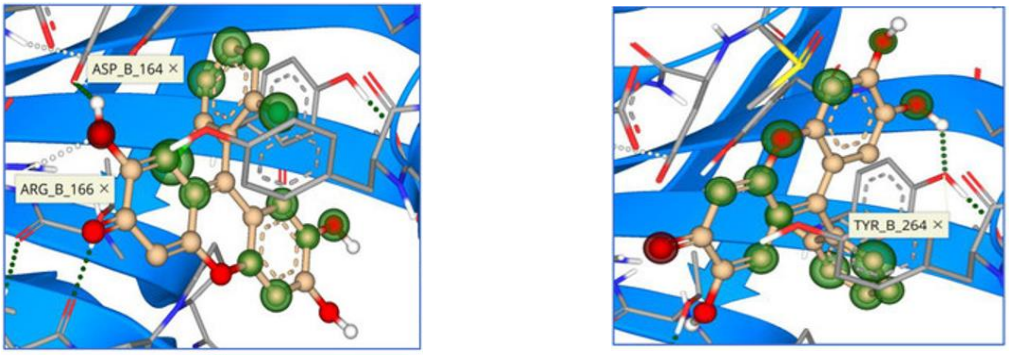

a) b)

Figure 13. Binding conformations and interacting amino acid residues of synthesized compounds 16 (a) and 17 (b) within papain-like protease, including HYDE-derived atomic contribution mapping (green circled atoms).

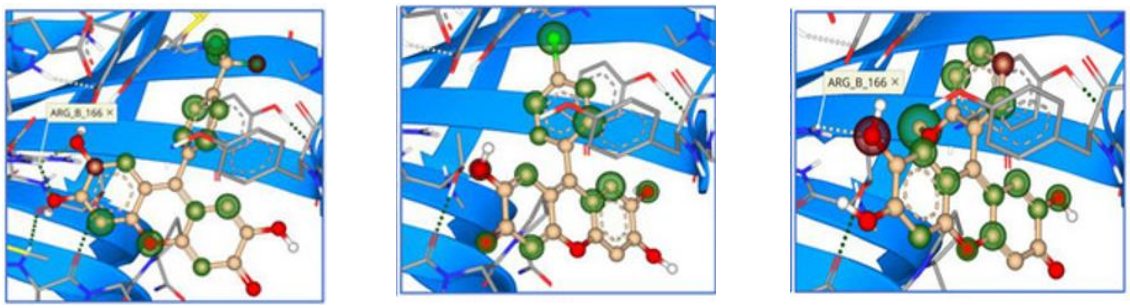

a) b) c)

Figure 14. Binding conformations and interacting amino acid residues of synthesized compounds 18 (a), 19 (b), and 20 (c) within papain-like protease, with HYDE energetic contribution visualization (green circled atoms).

Predicted binding affinities ranged from 0.171 to 0.286 mM **(Table 4),** confirming that the synthesized xanthene-3-one derivatives are the most effective PLpro inhibitors overall and reinforcing the conclusion that papain-like protease is a more druggable target. Interaction patterns were consistent with those observed for marine compounds, predominantly involving Asp 164, Arg 166, and Tyr 264 **(Figures 13 and 14).**

Differences in the structural organization of SARS-CoV-2 main protease (Mpro) and papain-like protease (PLpro) largely determine how amenable these enzymes are to pharmacological inhibition, particularly in terms of ligand accommodation and binding behavior. The Mpro enzyme is characterized by a compact and highly conserved catalytic pocket formed around a Cys145–His41 dyad. This relatively stable architecture supports adaptable ligand recognition and has therefore made Mpro a widely pursued target for small-molecule inhibitor development [58, 59]. In contrast, PLpro contains a more elaborate catalytic system (Cys111, His272, and Asp286) and possesses a broader, more conformationally adaptable binding region, which complicates structure-based inhibitor optimization [53]. Interestingly, the higher predicted binding strength observed for PLpro-directed compounds in this study is likely linked to this increased pocket size and structural plasticity, which allow ligands to establish more extensive and varied contacts.

While docking simulations are useful for generating initial hypotheses about ligand–protein recognition, their predictive capacity is limited by several methodological constraints. These include the inability to fully capture protein flexibility, the risk of over- or underestimating binding events, and the simplified treatment of solvation and entropic contributions. For this reason, docking outputs are generally considered preliminary and are ideally complemented by molecular dynamics simulations, binding free energy estimations, or experimental assays to confirm biological relevance.

Variability at the genetic level can significantly reshape the interactions between biomolecules and therapeutic compounds. Mutations may modify active site geometry, alter electrostatic environments, or disrupt key interaction networks, all of which can directly influence binding strength and drug effectiveness. This aspect is

particularly important in antiviral drug discovery, where evolving viral proteins can reduce drug sensitivity and contribute to the development of resistance.

The binding behavior of xanthene derivatives is highly dependent on the structural characteristics of the target protease. Differences in active site geometry and catalytic organization result in multiple interaction patterns across enzymes. These compounds typically stabilize within binding pockets through a combination of hydrogen bonding, hydrophobic contacts, and spatial complementarity. A recurring interaction pattern is observed with Mpro, where marine-derived xanthene compounds consistently form hydrogen bonds with His41, a crucial residue of the catalytic dyad responsible for enzymatic activity.

A structural comparison of binding orientations reveals that the top five marine-derived ligands adopt a nearly uniform pose within the Mpro active site **(Figure 15).** In contrast, synthesized compounds with similar core structures exhibit multiple and less consistent binding orientations **(Figure 16).**

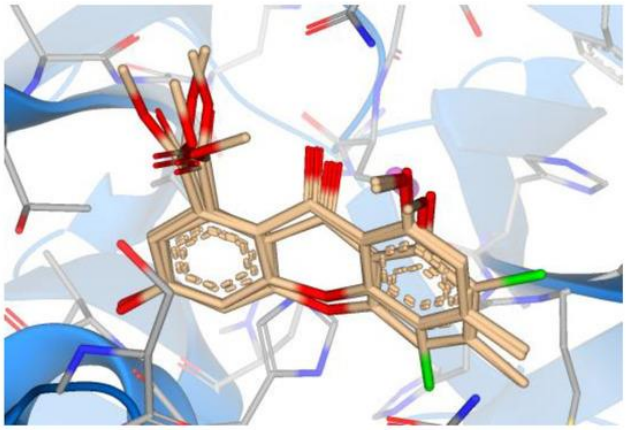

Figure 15. Superposition of the five highest-ranking marine compounds within the Mpro binding site.

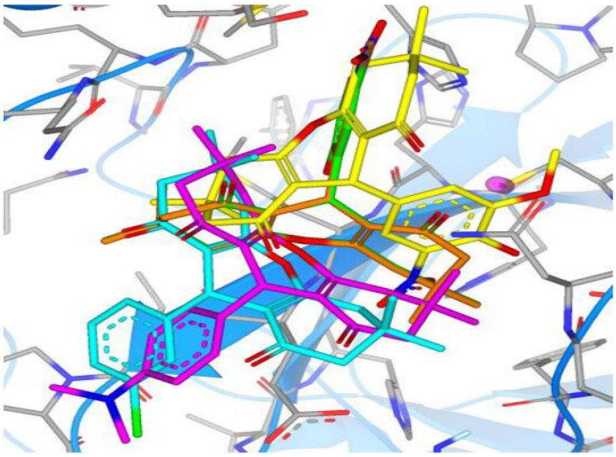

Figure 16. Superposition of the five highest-ranking synthesized compounds within the Mpro binding site (6—green, 7—orange, 8—magenta, 9—cyan, 10—yellow).

Within the synthesized set, compounds 6 and 7 share an almost identical binding configuration. A second shared orientation is observed for compounds 8 and 9. However, compound 10 (highlighted in yellow) **(Figure 16)** diverges markedly, adopting a distinct pose in which its 9-aryl substituent is oriented away from the catalytic pocket.

For PLpro, marine-derived compounds again demonstrate variability in binding orientations, consistent with their structural diversity **(Figure 17).** In contrast, synthesized xanthene-3-one derivatives show a more convergent behavior: four compounds align closely in the binding site, whereas compound 20 presents an inverted orientation relative to the others **(Figure 18).**

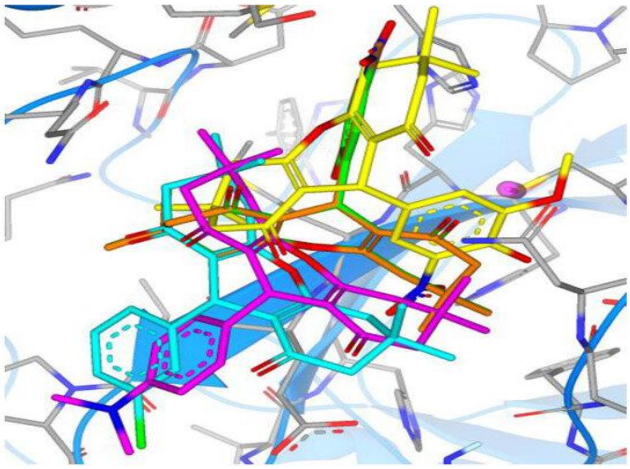

Figure 16. Superposition of the five highest-ranking synthesized compounds within the Mpro binding site (6—green, 7—orange, 8—magenta, 9—cyan, 10—yellow).

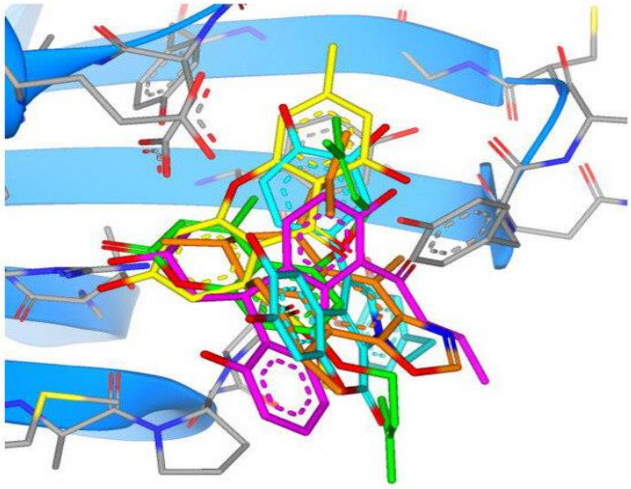

Figure 17. Superposition of the five highest-ranking marine compounds within the PLpro binding site (11—green, 12—orange, 13—magenta, 14—cyan, 15—yellow).

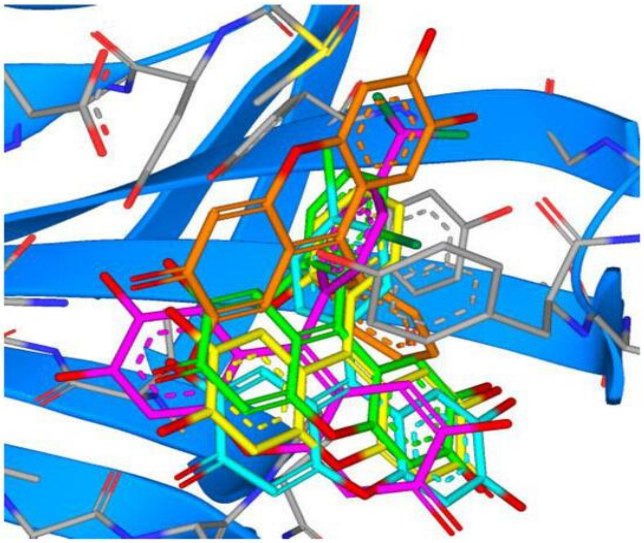

Figure 18. Superposition of the five highest-ranking synthesized compounds within the PLpro binding site (16—green, 17—orange, 18—magenta, 19—cyan, 20—yellow).

In early drug discovery, evaluating whether biologically active molecules may succeed as therapeutic agents relies heavily on physicochemical descriptors and pharmacokinetic modeling. A central early filter is membrane permeability, particularly intestinal absorption. One widely used framework is Lipinski's rule of five, which defines thresholds for passive oral uptake. According to this rule, compounds are more likely to be orally absorbed when they meet the following criteria: molecular weight below 500 g/mol, lipophilicity (logP) under 5, no more than 5 hydrogen bond donors, and no more than 10 hydrogen bond acceptors [60].

This rule has been expanded with additional descriptors that better capture molecular behavior. These include molar refractivity (40–130), topological polar surface area (TPSA ≤ 140 Å²), and fewer than 10 rotatable bonds (RB) [61, 62], which together reflect steric flexibility and permeability potential. Compounds satisfying these conditions are generally considered orally bioavailable, whereas violations of two or more parameters usually suggest limited passive diffusion across the intestinal wall.

Beyond absorption, lipophilicity-derived parameters also allow estimation of distribution behavior, metabolic processing, elimination, and toxicity risk profiles [61]. Among these, logD and logS are particularly relevant. LogD represents the balance between hydrophobic and hydrophilic properties of ionizable molecules at physiological pH (7.4), expressed as the octanol/water partition coefficient. LogS @ pH 7.4 refers to intrinsic aqueous solubility under physiological conditions (μM scale) for ionizable compounds.

Transport-related pharmacokinetics is further influenced by human intestinal absorption (HIA) and plasma protein binding (PPB) [63]. Compounds predicted to have ≥ 30% absorption are marked "+", while those below this threshold are labeled "−". Plasma protein binding is equally important for systemic exposure: molecules with > 90% binding are classified as "high", while those below 90% are considered "low". Increased protein binding reduces the fraction of free, pharmacologically active drug in circulation [64].

Blood–brain barrier (BBB) permeability is a critical determinant for compounds intended to act on the central nervous system [65, 66]. CYP2C9 pKi values estimate binding affinity to a metabolic enzyme involved in drug clearance pathways. CYP2D6 classification divides compounds into four affinity categories: low (<5), medium (5–6), high (6–7), and very high (> 7).

Another key pharmacokinetic factor is interaction with P-gp (MDR1/ABCB1), which mediates efflux transport and contributes to multidrug resistance. Prediction of P-gp substrate status indicates whether a compound is likely to be actively exported from cells.

Cardiotoxicity risk is evaluated by predicted inhibition of the human Ether-à-go-go-Related Gene (hERG) potassium channel, expressed in cardiac tissue; elevated pIC50 values may signal potential adverse cardiac effects.

For SARS-CoV-2 main protease, the top five marine-derived compounds showed favorable oral bioavailability profiles overall. Their logP values ranged from 2.93 to 3.86, and all remaining descriptors (molecular weight, hydrogen bond capacity, rotatable bonds, TPSA, and molar refractivity) remained within drug-likeness boundaries. As shown in **Table 1**, all compounds were predicted to have positive intestinal absorption, although plasma protein binding values were generally high.

Similarly, the five leading synthesized compounds targeting the main protease also satisfied oral bioavailability criteria. Their logP values were slightly elevated (3.88–5.00) but still within acceptable limits, and other parameters also met drug-likeness requirements. **Table 2** indicates that all compounds exhibited positive intestinal absorption.

For papain-like protease, the top five marine-origin compounds also demonstrated favorable pharmacokinetic profiles, with logP values ranging from 2.51 to 4.28, except for compound 7, which showed a higher logP of 6.46 **(Table 3).** Most compounds satisfied additional drug-likeness criteria, although compound 9 deviated, with six hydrogen bond donors and a TPSA of ~150 Å². Despite such deviations, partial rule violations do not necessarily prevent acceptable oral bioavailability. As shown in **Table 3**, all compounds except compound 9 exhibited positive intestinal absorption, while plasma protein binding varied across the group.

The synthesized compounds tested against papain-like protease also showed good oral bioavailability potential, with logP values ranging from 3.23 to 3.95. The remaining physicochemical descriptors remained within acceptable limits for drug-likeness. According to **Table 4,** all compounds displayed positive intestinal absorption, while plasma protein binding was generally high except for compound 20.

Although the identified inhibitors for SARS-CoV-2 Mpro and PLpro may extend to other coronaviruses due to conserved protease architecture, differences in sequence variation, structural dynamics, and host interaction strategies can significantly alter their pharmacological relevance. In particular, strong PLpro binding observed in SARS-CoV-2 may not directly translate to other coronaviruses if structural divergence or alternative immune

modulation mechanisms are present. Therefore, while these results provide a useful foundation for broad-spectrum antiviral development, additional comparative studies across coronavirus families are required to refine inhibitor design and evaluate cross-species applicability.

The characterization of ligand interactions within the active sites of SARS-CoV-2 main protease and papain-like protease, as obtained through docking analyses, provides an important basis for prioritizing lead candidates with potential biological activity in experimental systems. Such computational evaluations enable ranking compounds by predicted binding strength and inferred pharmacological behavior, thereby selecting the most promising inhibitors for subsequent in vitro validation against target enzymes.

Insights derived from molecular docking of Mpro and PLpro are also highly relevant for downstream translational stages, including in vivo evaluation and clinical development. These structural interpretations support the identification and refinement of lead molecules, improving their potency, selectivity, and safety profiles before experimental testing. In this way, computational screening serves as an initial filter, accelerating antiviral drug discovery and enabling the faster development of therapeutic options for COVID-19 and related coronavirus diseases.

The present investigation expands the current understanding of SARS-CoV-2 protease inhibition by introducing previously unexplored chemical scaffolds, specifically xanthene, coumarin, and benzoxazole derivatives originating from both marine sources and synthetic libraries. These molecules exhibit diverse binding orientations and inhibitory mechanisms, particularly against both Mpro and PLpro enzymes. Moreover, the study strengthens the broader concept of multi-target antiviral development. The combination of marine-derived chemistry with synthetic compound libraries creates additional opportunities for lead identification and enhances current knowledge of protease inhibition strategies, supporting future drug development efforts.

Conclusion

Although the global situation has shifted from a pandemic phase toward endemic circulation, SARS-CoV-2 continues to circulate widely and remains a persistent public health concern. Ongoing viral evolution results in the continuous emergence of new variants, sustaining transmission dynamics. Despite extensive global efforts in vaccination, therapeutic development, and clinical management, the public health burden remains substantial. One major limitation in treatment strategies is the scarcity of orally available antiviral agents. Consequently, there is a continuing and urgent demand for broad-spectrum antiviral compounds capable of addressing both current and future coronavirus outbreaks.

In this study, molecular docking was used to evaluate the interactions of 118 marine-derived compounds and 92 previously synthesized molecules with the SARS-CoV-2 main protease and papain-like protease. Screening results identified leading candidates from xanthene, benzoxazole, and coumarin chemical classes. Overall, marine-origin compounds demonstrated slightly improved inhibitory potential, whereas synthesized molecules showed comparable binding affinities, with the strongest candidates falling within the 0.2–0.4 mM range. Across both natural and synthetic libraries, xanthene-based structures emerged as the most promising chemical framework for further optimization.

Between the two viral targets studied, PLpro appeared to be more druggable than Mpro. All top-performing compounds met multiple drug-likeness criteria, suggesting favorable oral bioavailability and reduced toxicity. Compared with the FDA-approved Mpro inhibitor nirmatrelvir and the experimental PLpro inhibitor Jun12682, several identified compounds also performed favorably.

The structural insights obtained from docking simulations of SARS-CoV-2 proteases (Mpro and PLpro) provide a valuable foundation for subsequent in vivo and clinical investigations. These findings facilitate the selection of optimized lead compounds, supporting improvements in efficacy and safety profiles, and enhancing the likelihood of clinical success. By integrating computational predictions early in the drug discovery process, the process can be made more efficient, thereby accelerating the development of antiviral therapies not only for COVID-19 but also for other coronavirus-related diseases.

Overall, this expanded analysis provides meaningful comparative insight into the binding behavior of marine-derived and synthetic compounds across xanthene, coumarin, and benzoxazole scaffolds, highlighting several promising candidates that warrant further in vitro and in vivo evaluation.

Acknowledgments: This research was supported by grant number 27-02-11-41250-15/21 from the Ministry of Science, Higher Education, and Youth of Canton Sarajevo.

Conflict of Interest: None

Financial Support: None

Ethics Statement: None

References

1. Fan H, Qin S, Cui Y. Emergence and characterization of the SARS-CoV-2 JN.1 variant: global prevalence and implications for public health. Zoonoses. 2024;4:994.
2. Li Q, Guan X, Wu P, Wang X, Zhou L, Tong Y, et al. Early transmission dynamics in Wuhan, China, of novel coronavirus-infected pneumonia. N Engl J Med. 2020;382:1199-207.
3. World Health Organization. Number of COVID-19 cases reported to WHO (cumulative total). Available from: https://data.who.int/dashboards/covid19/cases?n=o
4. World Health Organization. Number of COVID-19 deaths reported to WHO (cumulative total). Available from: https://data.who.int/dashboards/covid19/deaths?n=o
5. Carabelli AM, Peacock TP, Thorne LG, Harvey WT, Hughes J, Peacock SJ, et al. SARS-CoV-2 variant biology: immune escape, transmission and fitness. Nat Rev Microbiol. 2023;21:162-77.
6. Javed S, Farhan BA, Shabbir M, Tahseen A, Ahmedah HT, Moga M. Morphology, pathogenesis, genome organization, and replication of coronavirus (COVID-19). In: The COVID-19 Pandemic. 1st ed. Palm Bay (FL): Apple Academic Press; 2022. p. 3-43.
7. Zmasek CM, Lefkowitz EJ, Niewiadomska A, Scheuermann RH. Genomic evolution of the Coronaviridae family. Virology. 2022;570:123-33.
8. Shi Z, Hu B, Wang LF. Zoonotic origin and evolution of SARS coronavirus. In: Genetics and Evolution of Infectious Diseases. 3rd ed. Amsterdam: Elsevier; 2024. p. 841-61.
9. Scheller C, Krebs F, Minkner R, Astner I, Gil-Moles M, Wätzig H. Physicochemical properties of SARS-CoV-2 for drug targeting, virus inactivation and attenuation, vaccine formulation and quality control. Electrophoresis. 2020;41:1137-51.
10. Kumar R, Srivastava Y, Muthuramalingam P, Singh SK, Verma G, Tiwari S, et al. Understanding mutations in human SARS-CoV-2 spike glycoprotein: a systematic review and meta-analysis. Viruses. 2023;15:856.
11. Markov PV, Ghafari M, Beer M, Lythgoe K, Simmonds P, Stilianakis NI, et al. The evolution of SARS-CoV-2. Nat Rev Microbiol. 2023;21:361-79.
12. Singh D, Yi SV. On the origin and evolution of SARS-CoV-2. Exp Mol Med. 2021;53:537-47.
13. Chakraborty C, Bhattacharya M, Dhama K. SARS-CoV-2 vaccines, vaccine development technologies, and significant efforts in vaccine development during the pandemic: the lessons learned might help to fight against the next pandemic. Vaccines (Basel). 2023;11:682.
14. Jadhav P, Huang B, Osipiuk J, Zhang X, Tan H, Tesar C, et al. Structure-based design of SARS-CoV-2 papain-like protease inhibitors. Eur J Med Chem. 2024;264:116011.
15. Kakavandi S, Zare I, VaezJalali M, Dadashi M, Azarian M, Akbari A, et al. Structural and nonstructural proteins in SARS-CoV-2: potential aspects to COVID-19 treatment or prevention of progression of related diseases. Cell Commun Signal. 2023;21:110.
16. Onyango OH. In silico models for anti-COVID-19 drug discovery: a systematic review. Adv Pharmacol Pharm Sci. 2023;2023:4562974.
17. Ghosh AK, Shahabi D, Imhoff ME, Kovela S, Sharma A, Hattori SI, et al. SARS-CoV-2 papain-like protease (PLpro) inhibitory and antiviral activity of small molecule derivatives for drug leads. Bioorg Med Chem Lett. 2023;96:129489.
18. Sanders BC, Pokhrel S, Labbe AD, Mathews II, Cooper CJ, Davidson RB, et al. Potent and selective covalent inhibition of the papain-like protease from SARS-CoV-2. Nat Commun. 2023;14:1733.

19. Funk LM, Poschmann G, Rabe von Pappenheim F, Chari A, Stegmann KM, Dickmanns A, et al. Multiple redox switches of the SARS-CoV-2 main protease in vitro provide opportunities for drug design. Nat Commun. 2024;15:411.
20. Melano I, Lo Y, Su W. Characterization of host substrates of SARS-CoV-2 main protease. Front Microbiol. 2023;14:1251705.
21. Chan HH, Brewitz L, Lukacik P, Strain-Damerell C, Walsh MA, Schofield CJ, et al. Studies on the selectivity of the SARS-CoV-2 papain-like protease reveal the importance of the P2′ proline of the viral polyprotein. RSC Chem Biol. 2024;5:117-30.
22. Citarella A, Dimasi A, Moi D, Passarella D, Scala A, Piperno A, et al. Recent advances in SARS-CoV-2 main protease inhibitors: from nirmatrelvir to future perspectives. Biomolecules. 2023;13:1339.
23. Waqas M, Ullah S, Halim SA, Rehman NU, Ali A, Jan A, et al. Targeting papain-like protease by natural products as novel therapeutic potential SARS-CoV-2. Int J Biol Macromol. 2024;258:128812.
24. Banerjee P, Mandhare A, Bagalkote V. Marine natural products as a source of new drugs: an updated patent review. Expert Opin Ther Pat. 2022;32:317-63.
25. Chhetri BK, Tedbury PR, Sweeney-Jones AM, Mani L, Soapi K, Manfredi C, et al. Marine natural products as leads against SARS-CoV-2 infection. J Nat Prod. 2022;85:657-65.
26. Zaporozhets TS, Besednova NN. Biologically active compounds from marine organisms in the strategies for combating coronaviruses. AIMS Microbiol. 2020;6:470-86.
27. Abdallah HM, El-Halawany AM, Sirwi A, El-Araby AM, Mohamed GA, Ibrahim SR, et al. Repurposing of some natural product isolates as SARS-CoV-2 main protease inhibitors via in vitro cell-free and cell-based antiviral assessments and molecular modeling approaches. Pharmaceuticals (Basel). 2021;14:213.
28. Wang SC, Chen Y, Wang YC, Wang WJ, Yang CS, Tsai CL, et al. Tannic acid suppresses SARS-CoV-2 as a dual inhibitor of the viral main protease and the cellular TMPRSS2 protease. Am J Cancer Res. 2020;10:4538-55.
29. White KM, Rosales R, Yildiz S, Kehrer T, Miorin L, Moreno E, et al. Plitidepsin has potent preclinical efficacy against SARS-CoV-2 by targeting the host protein eEF1A. Science. 2021;371:926-31.
30. Minagawa K, Kouzuki S, Yoshimoto J, Kawamura Y, Tani H, Iwata T, et al. Stachyflin and acetylstachyflin, novel anti-influenza A virus substances, produced by Stachybotrys sp. RF-7260 I. Isolation, structure elucidation and biological activities. J Antibiot (Tokyo). 2002;55:155-64.
31. Tsujii S, Rinehart KL, Gunasekera SP, Kashman Y, Cross SS, Lui MS, et al. Topsentin, bromotopsentin, and dihydrodeoxybromotopsentin: antiviral and antitumor bis(indolyl)imidazoles from Caribbean deep-sea sponges of the family Halichondriidae. Structural and synthetic studies. J Org Chem. 1988;53:5446-53.
32. Ishida J, Wang HK, Oyama M, Cosentino ML, Hu CQ, Lee KH. Anti-AIDS agents. 46. Anti-HIV activity of harman, an anti-HIV principle from Symplocos setchuensis, and its derivatives. J Nat Prod. 2001;64:958-60.
33. Kim DE, Min JS, Jang MS, Lee JY, Shin YS, Park CM, et al. Natural bis-benzylisoquinoline alkaloids-tetrandrine, fangchinoline, and cepharanthine, inhibit human coronavirus OC43 infection of MRC-5 human lung cells. Biomolecules. 2019;9:696.
34. Cheng PNL, Chiang LC, Lin CC. Antiviral effects of saikosaponins on human coronavirus 229E in vitro. Clin Exp Pharmacol Physiol. 2006;33:612-6.
35. Hong S, Seo SH, Woo SJ, Kwon Y, Song M, Ha NC. Epigallocatechin gallate inhibits the uridylate-specific endoribonuclease Nsp15 and efficiently neutralizes the SARS-CoV-2 strain. J Agric Food Chem. 2021;69:5948-54.
36. Ding Y, Zhu X, Hao L, Zhao M, Hua Q, An F. Bioactive indolyl diketopiperazines from the marine-derived endophytic Aspergillus versicolor DY180635. Mar Drugs. 2020;18:338.
37. Cheohen CF, Esteves ME, da Fonseca TS, Leal CM, Assis FD, Campos MF, et al. In silico screening of phenylethanoid glycosides, a class of pharmacologically active compounds as natural inhibitors of SARS-CoV-2 proteases. Comput Struct Biotechnol J. 2023;21:1461-72.
38. Vegad UG, Gajjar ND, Nagar PR, Chauhan SP, Pandya DJ, Dhameliya TM. In silico screening, ADMET analysis and MD simulations of phytochemicals of Onosma bracteata Wall. as SARS-CoV-2 inhibitors. 3 Biotech. 2023;13:221.
39. Mohapatra PK, Chopdar KS, Dash GC, Mohanty AK, Raval MK. In silico screening and covalent binding of phytochemicals of Ocimum sanctum against SARS-CoV-2 (COVID-19) main protease. J Biomol Struct Dyn. 2023;41:435-44.

40. Hu C. Marine natural products and human immunity: novel biomedical resources for anti-infection of SARS-CoV-2 and related cardiovascular disease. Nat Prod Bioprospect. 2024;14:12.
41. Salihović M, Osmanović A, Špirtović-Halilović S, Roca S, Meščić A, Vujisić L, et al. Synthesis, structural, conformational and DFT studies of N-3 and O-4 alkylated regioisomers of 5-(hydroxypropyl) pyrimidine. J Mol Struct. 2015;1091:170-6.
42. Špirtović-Halilović S, Veljović E, Salihović M, Osmanović A, Šapčanin A, Softić D, et al. Synthesis, microbiological activity and in silico investigation for some synthesized coumarin derivatives. Croat Chem Acta. 2020;93:23-31.
43. Bilajac E, Osmanović A, Glamočlija U, Veljović E, Imamović B, Bečić E, et al. Synthesis, in silico study and antitumor activity of coumarin compounds in lymphoma cells. Farmacia. 2023;71:1263-73.
44. Završnik D, Špirtović-Halilović S, Softić D. Synthesis, structure and antibacterial activity of 3-substituted derivatives of 4-hydroxycoumarin. Period Biol. 2011;113:93-7.
45. Veljović E, Špirtović-Halilović S, Muratović S, Valek Žulj L, Roca S, Trifunović S, et al. 9-Aryl substituted hydroxylated xanthen-3-ones: synthesis, structure and antioxidant potency evaluation. Croat Chem Acta. 2015;88:121-7.
46. Veljović E, Špirtović-Halilović S, Muratović S, Osmanović A, Badnjević A, Gurbeta L, et al. Artificial neural network and docking study in design and synthesis of xanthenes as antimicrobial agents. In: Badnjević A, editor. CMBEBIH 2017 Proceedings of the International Conference on Medical and Biological Engineering. Singapore: Springer; 2017. p. 617-26.
47. Zukić S, Veljović E, Špirtović-Halilović S, Muratović S, Osmanović A, Trifunović S, et al. Antioxidant, antimicrobial and antiproliferative activities of synthesized 2,2,5,5-tetramethyl-9-aryl-3,4,5,6,7,9-hexahydro-1H-xanthene-1,8(2H)-dione derivatives. Croat Chem Acta. 2018;91:1-9.
48. Veljović E, Špirtović-Halilović S, Muratović S, Osmanović A, Novaković I, Trifunović S, et al. Synthesis and biological evaluation of xanthen-1,8-dione derivatives. Bull Chem Technol Bosnia Herzegovina. 2018;51:13-8.
49. Glamočlija U, Padhye S, Špirtović-Halilović S, Osmanović A, Veljović E, Roca S, et al. Synthesis, biological evaluation and docking studies of benzoxazoles derived from thymoquinone. Molecules. 2018;23:3297.
50. Bilajac E, Glamočlija U, Osmanović A, Mahmutović L, Sezer A, Roca S, et al. Analysis of antitumor potential of xanthene compounds in lymphoma cells. Croat Chem Acta. 2023;96:59-68.
51. Spirtović-Halilović S, Salihović M, Osmanović A, Veljović E, Rahić O, Mahmutović E, et al. In silico study of microbiologically active benzoxazole derivatives. Indian J Pharm Sci. 2023;85:767-77.
52. Owen DR, Allerton CM, Anderson AS, Aschenbrenner L, Avery M, Berritt S, et al. An oral SARS-CoV-2 Mpro inhibitor clinical candidate for the treatment of COVID-19. Science. 2021;374:1586-93.
53. Tan B, Zhang X, Ansari A, Jadhav P, Tan H, Li K, et al. Design of a SARS-CoV-2 papain-like protease inhibitor with antiviral efficacy in a mouse model. Science. 2024;383:1434-40.
54. Schneider N, Lange G, Hindle S, Klein R, Rarey M. A consistent description of HYdrogen bond and DEhydration energies in protein-ligand complexes: methods behind the HYDE scoring function. J Comput Aided Mol Des. 2013;27:15-29.
55. Reulecke I, Lange G, Albrecht J, Klein R, Rarey M. Towards an integrated description of hydrogen bonding and dehydration: decreasing false positives in virtual screening with the HYDE scoring function. ChemMedChem. 2008;3:885-97.
56. Rarey M, Kramer B, Lengauer T, Klebe G. A fast flexible docking method using an incremental construction algorithm. J Mol Biol. 1996;261:470-89.
57. Gastreich M, Lilienthal M, Briem H, Claussen H. Ultrafast de novo docking combining pharmacophores and combinatorics. J Comput Aided Mol Des. 2007;20:717-34.
58. Duan Y, Wang H, Yuan Z, Yang H. Structural biology of SARS-CoV-2 Mpro and drug discovery. Curr Opin Struct Biol. 2023;82:102667.
59. Zagórska A, Czopek A, Fryc M, Jończyk J. Inhibitors of SARS-CoV-2 main protease (Mpro) as anti-coronavirus agents. Biomolecules. 2024;14:797.
60. Lipinski CA, Lombardo F, Dominy BW, Feeney PJ. Experimental and computational approaches to estimate solubility and permeability in drug discovery and development settings. Adv Drug Deliv Rev. 1997;23:3-25.
61. Veber DF, Johnson SR, Cheng HY, Smith BR, Ward KW, Kopple KD. Molecular properties that influence the oral bioavailability of drug candidates. J Med Chem. 2002;45:2615-23.

62. Congreve M, Carr R, Murray C, Jhoti H. A rule of three for fragment-based lead discovery? Drug Discov Today. 2003;8:876-7.
63. Yan A, Wang Z, Cai Z. Prediction of human intestinal absorption by GA feature selection and support vector machine regression. Int J Mol Sci. 2008;9:1961-76.
64. Ghafourian T, Amin Z. QSAR models for the prediction of plasma protein binding. Bioimpacts. 2013;3:21-7.
65. Daneman R, Prat A. The blood-brain barrier. Cold Spring Harb Perspect Biol. 2015;7:a020412.
66. Summerfield SG, Read K, Begley DJ, Obradovic T, Hidalgo IJ, Coggon S, et al. Central nervous system drug disposition: the relationship between in situ brain permeability and brain free fraction. J Pharmacol Exp Ther. 2007;322:205-13.